Solar Energy 171 (2018) 728–739

Contents lists available at ScienceDirect

Solar Energy

journal homepage: www.elsevier.com/locate/solener

# Optimum sizing of the inverter for maximizing the energy yield in state-of-the-art high-concentrator photovoltaic systems

Pedro J. Pérez-Higueras[a], Florencia M. Almonacid[a], Pedro M. Rodrigo[b,*], Eduardo F. Fernández[a]

[a] Centre for Advanced Studies in Energy and Environment (CEAEMA), IDEA Solar Energy Research Group, Electronics and Automation Engineering Department, University of Jaén, Las Lagunillas Campus, Jaén 23071, Spain

[b] Universidad Panamericana. Facultad de Ingeniería. Josemaría Escrivá de Balaguer 101, Aguascalientes, Aguascalientes 20290, Mexico

ARTICLE INFO

*Keywords:*
Concentrator photovoltaics
Inverter sizing
Meteorological databases
Photovoltaic model

ABSTRACT

The sizing of the inverter in comparison to the rated capacity of the photovoltaic generator is investigated for high-concentrator photovoltaic (HCPV) systems. An HCPV module of typical characteristics is modelled and parameterized, taking into account direct normal irradiance (DNI), ambient temperature, air mass and aerosol optical depth as atmospheric inputs, while the DC losses of the HCPV generator are allowed to vary in the ranges reported in the literature. A set of 80 commercial inverters are analysed to obtain the typical efficiency curves of state-of-the-art low-, medium-, and high-efficiency inverters. Four locations worldwide with high annual DNI levels and different average values of the weather variables influencing HCPV performance are studied. Results show that the inverter can be sized between 84% and 112% of the rated capacity of the HCPV generator at Concentrator Standard Test Conditions depending on the scenario considered for maximizing the final energy yield of the system. The proposed methodology uses analytical equations, all the model parameters are provided and justified and atmospheric inputs are obtained from meteorological databases in order to make the application easy regarding its use in other locations where the climate data is available.

## 1. Introduction

The basic concept of the concentrator photovoltaic (CPV) technology consists in the use of optical devices to concentrate the sunlight onto photovoltaic (PV) cells. These systems incorporate different elements such as CPV modules, sun trackers and grid-connected inverters, with many possible different configurations (Muñoz et al., 2015). The present work focuses on high-concentrator photovoltaic (HCPV) systems, characterized by a geometric concentration ratio in the range between 100 and 2000 suns (Pérez-Higueras et al., 2011; Shanks et al., 2016). In HCPV systems, the HCPV modules are mounted on two-axis sun trackers because the optical elements must be always pointing to the sun in order to concentrate the sunlight on a very small area, where the solar cells (usually multi-junction III-V solar cells) are placed. In this way, HCPV systems only exploit the direct component of the solar radiation and are appropriate in locations with high annual levels of direct normal irradiance (*DNI*). HCPV technology is of big interest nowadays as an emerging renewable energy technology, which began the commercialization stage recently and has greater presence in the market than the rest of CPV technologies (Philipps et al., 2016). These systems have demonstrated the highest conversion efficiencies of terrestrial PV applications and the forecast of HCPV installed capacity for 2020 is above 1 GWp (Global Data, 2015). However, at present, the cost per generated kWh of electricity is higher for HCPV systems than for conventional PV systems (Talavera et al., 2016). This implies that a careful selection of all the system components must be carried out in the design of HCPV facilities in order to optimise the energetic and economic performance of the projects. One of the aspects to be considered is finding an adequate matching between the inverter nominal power and the PV array peak power. This allows the average annual inverter efficiency and, thus, the final energy yield of the system to be maximized.

Even when many studies in the literature analyse the sizing of inverters for conventional PV systems, as shown in Section 2, and taking into account that all of these studies could be taken into consideration as a reference for adequate choosing the size of inverters in HCPV systems, it is important to highlight that the sizing task in HCPV is inherently different than the sizing in conventional PV systems. This is because of two main reasons: first, the main input regarding atmospheric variables in HCPV is the *DNI*, instead of the plane-of-array global irradiance considered in conventional PV systems. The annual distribution of *DNI* for a particular site is different than the global

* Corresponding author.
*E-mail address:* prodrigo@up.edu.mx (P.M. Rodrigo).

https://doi.org/10.1016/j.solener.2018.07.013
Received 22 May 2018; Received in revised form 28 June 2018; Accepted 6 July 2018

**Nomenclature**

| | |
|---|---|
| $AM$ | air mass |
| $AM_u$ | threshold air mass coefficient |
| $AOD_{550}$ | aerosol optical depth at 550 nm |
| $AOD_{550,u}$ | threshold aerosol optical depth at 550 nm coefficient |
| $DNI$ | direct normal irradiance [W m$^{-2}$] |
| $DNI_A$ | annual direct normal irradiation [kWh m$^{-2}$] |
| $DNI_{CSTC}$ | direct normal irradiance at concentrator standard test conditions [W m$^{-2}$] |
| $I_{mpp}$ | maximum power point current of an HCPV module at concentrator standard test conditions [A] |
| $I_{sc}$ | short-circuit current of an HCPV module at concentrator standard test conditions [A] |
| $L_0$ | inverter constant self-consumption loss coefficient |
| $L_1$ | inverter increasing linearly with power loss coefficient |
| $L_2$ | inverter increasing linearly with the square of power loss coefficient |
| $L_{AC}$ | AC loss coefficient of the HCPV system |
| $L_{DC}$ | DC loss coefficient of the HCPV generator |
| $P_{gen,CSTC}$ | HCPV generator rated power at concentrator standard test conditions [W] |
| $p_{in}$ | inverter input DC power normalized to the inverter nominal AC power |
| $P_{inv,nom}$ | inverter nominal power [W] |
| $P_{max}$ | maximum power of an HCPV module at concentrator standard test conditions [W] |
| $p_{mod,MPP}$ | HCPV module maximum power normalized to 1 kWp of nominal power rated at concentrator standard test conditions |
| $PR$ | performance ratio of the HCPV system |
| $p_{sys}$ | output power of an HCPV system per kWp of installed power rated at concentrator standard test conditions |
| $PW$ | precipitable water [cm] |
| $R^2$ | correlation coefficient of a linear regression |
| $R_{th}$ | thermal resistance of an HCPV module [°C m$^2$ W$^{-1}$] |
| $SMR$ | spectral matching ratio |
| $SR$ | sizing ratio |
| $SR_o$ | optimum sizing ratio under the condition that the HCPV generator DC loss coefficient equals zero |
| $SR_{opt}$ | optimum sizing ratio that maximizes the annual energy yield |
| $T_{air}$ | ambient temperature [°C] |
| $T_{cell}$ | cell operating temperature inside an HCPV module [°C] |
| $T_{cell,CSTC}$ | cell temperature at concentrator standard test conditions [°C] |
| $V_{mpp}$ | maximum power point voltage of an HCPV module at concentrator standard test conditions [V] |
| $V_{oc}$ | open-circuit voltage of an HCPV module at concentrator standard test conditions [V] |
| $Y_f$ | final annual energy yield of the HCPV system [kWh kWp$^{-1}$] |
| $\delta$ | coefficient of variation of HCPV module maximum power with temperature [°C$^{-1}$] |
| $\Delta SR$ | per unit variation of the optimum sizing ratio with the HCPV generator DC loss coefficient |
| $\varepsilon$ | coefficient of variation of HCPV module maximum power with air mass |
| $\eta_{inv}$ | global efficiency of an inverter |
| $\eta_{max}$ | maximum operating efficiency of an inverter |
| $\varphi$ | coefficient of variation of HCPV module maximum power with aerosol optical depth at 550 nm |

irradiance distribution, and hence, the optimum sizing of the inverters is not necessarily the same for HCPV than for conventional PV. Moreover, we can find two locations with a similar global irradiance distribution, but they can differ in the *DNI* distribution because of different diffuse irradiance characteristics due to different cloud conditions and/or amount of aerosols in the atmosphere. This means that these two locations would verify a similar optimum inverter size for conventional systems, while they would require different optimal inverter sizes when considering HCPV systems. Second, the electrical behaviour of HCPV systems differs from that of conventional systems, due to the use of optical elements, multi-junction III-V solar cells, heat exchangers, sun trackers, etc. This implies that the models for the electrical characterization of HCPV systems are different than those of conventional systems (Rodrigo et al., 2013, 2014) and, thus, the procedures to optimise the inverter size are also different. Taking into account the above, it is evident that the sizing results obtained with conventional methods are not directly applicable to the HCPV technology and they should only be considered as a first approximation to the problem. Therefore, the development of new methods adapted to the peculiarities of the HCPV technology is required for the design of these kinds of installations.

In this paper, we analyse the optimum inverter size that maximizes the annual energy yield in HCPV systems. The HCPV systems under analysis use point-focus Fresnel lenses and triple-junction GaInP/GaInAs/Ge solar cells with a geometric concentration ratio of 550x and can be considered representative of the most typical HCPV technology installed nowadays. An extensive analysis of 80 commercial inverter datasheets was carried out to obtain general valid conclusions for the state-of-the-art inverter technology. Four locations worldwide with high levels of *DNI* and different atmospheric characteristics were considered in the analysis in order to show the influence of the local climate on the sizing of HCPV systems. Also, a discussion on the influence of the DC system losses, which can vary significantly from one HCPV system to another, in the optimum inverter sizing is presented. It is the aim of the authors to offer a complete study that covers scenarios as general as possible with respect to the existing technology of HCPV generators and inverters and, thus, can be used as a reference for HCPV system designers.

This study presents several novelties when compared to the literature review on inverter sizing for HCPV presented in Section 2. For the first time, the influence of aerosols on the HCPV generator output is considered in the analysis. Aerosols cause an increase of the diffuse component of the solar radiation and an appreciable decrease of the *DNI* (Fernández et al., 2016a; Rodrigo et al., 2017). In addition, it is worth mentioning that HCPV generators based on multi-junction solar cells are strongly affected by changes in the direct sunlight spectrum because of the internal series connection of different subcells with different spectral absorption bands (Domínguez et al., 2013; Rodrigo et al., 2017). Among the atmospheric parameters that influence the direct sunlight spectrum, the aerosol optical depth (*AOD*) has a far from negligible influence on the spectrum and, thus, on the electrical response of an HCPV generator, as was shown in different papers (Eltbaakh et al., 2012; Fernández et al., 2014a, 2016a; Núñez et al., 2016). However, previous studies neglected this influence in the sizing of HCPV systems (Chen and Melia, 2011; Martínez et al., 2016). In this study, this influence is considered and four locations with different average values of the atmospheric parameters influencing the solar spectrum, both for air mass (*AM*) and *AOD*, are evaluated. Another improvement with respect to the reviewed works is that, while the previous research considered specific types of inverters, in this study up to 80 commercial inverter datasheets have been analysed to obtain general valid conclusions for the state-of-the-art inverter technology. This analysis has allowed modelling the behaviour of typical low-, medium- and high-efficiency inverters present in the market nowadays, and differentiating the sizing ratio for each one of these inverter

categories. Thus, the results of the study can be considered more general and useful for the HCPV system designers than those presented in previous work (Chen and Melia, 2011; Martínez et al., 2016). Moreover, the developed methodology consists in analytical equations and all the model parameters are provided, so that we have facilitated the application of this methodology to other researchers and PV designers without the need of specific software or complex algorithms difficult to implement, with the only requirement being to have available meteorological data for the site under analysis.

The paper is structured as follows: in Section 2, the concept of Sizing Ratio is defined and a background of related works is presented; in Section 3, the proposed HCPV system modelling is described; in Section 4, the model parameters are justified and a discussion on the analysis of 80 commercial inverter datasheets is presented; in Section 5, the locations considered for the analysis are defined together with the climatic characteristics of each one and the source of the atmospheric data; Section 6 presents the results of the study, including the discussion on the histograms of DC power obtained in each location, on the optimum Sizing Ratio and on the sensitivity to the different possible levels of DC losses; finally, Section 7 details the conclusions of the study. An Appendix A is included that lists the commercial inverter models considered in the analysis.

## 2. Sizing ratio and related works

The instantaneous efficiency of a given inverter depends on the ratio of the actual inverter output power to its nominal power. This ratio is determined by the atmospheric conditions, the technological characteristics of the connected PV arrays and the inverter size with respect to the array size. Thus, designers have the opportunity to optimise the average annual inverter efficiency for a specific climate and PV technology just searching for an adequate relation between the inverter nominal power and the array peak power. In the present study, this relation is quantified by the Sizing Ratio (*SR*), which is defined as:

$$SR = P_{inv,nom}/P_{gen,CSTC} \quad (1)$$

where $P_{inv,nom}$ is the inverter nominal power and $P_{gen,CSTC}$ is the rated power of the HCPV generator connected to the inverter at Concentrator Standard Test Conditions (CSTC). These conditions are specified in the IEC 62670-1 standard and correspond to a *DNI* of 1000 W/m$^2$, a cell temperature of 25 °C and an AM1.5d standard spectrum (IEC 62670-1:2013, 2013). High values of *SR* (oversized inverters) have as a consequence that the inverters operate for prolonged periods of time at low load condition, which reduces the instantaneous inverter efficiency and therefore, the annual energy yield. This effect is corrected as the *SR* decreases, which implies an increase in the annual energy. However, this increase has a limit given by the prevalence of the so called "clipping" of the inverters, i.e. the limitation of the output power to the inverter nominal power. Low values of *SR* (undersized inverters) motivate the inverters to limit the output power to their nominal power in the periods of high irradiance. Thus, there is a point from which lowering the *SR* implies lowering the final energy yield. As a result, there is an optimum for *SR* that maximizes the energy harvesting. In addition to this, the lower the *SR*, the lower the inverter investment costs, so that the *SR* design parameter has implications both in the energy generated and in the project profitability.

The inverter sizing has been widely analysed in the literature for conventional flat-plate PV systems. One of the first studies goes back to 1992 covering the European geography and 35 inverter models (Jantsch et al., 1992). Authors found that the optimum *SR* to maximize energy harvesting varied between 0.85 and 1.00 for South-Europe, between 0.75 and 0.90 for Central-Europe and between 0.65 and 0.80 for North-Europe. From this study, many authors have gone deeper into the subject by analysing conventional PV technologies. Basically, the studies can be grouped in two categories: those that go after maximizing the annual energy yield of the system (energetic analysis) (Macagnan and Lorenzo, 1992; van der Borg and Burgers, 2003; Burger and Rüther, 2006; Macedo and Zilles, 2007; Notton et al., 2010; Demoulias, 2010; Velasco et al., 2010; Hussin et al., 2012; Luoma et al., 2012; Camps et al., 2015; Rodrigo et al., 2016a) and those that go after optimising economic parameters, such as the levelised cost of electricity or the internal rate of return (economic analysis) (Peippo and Lund, 1994a, 1994b; Keller and Affolter, 1995; Nofuentes and Almonacid, 1999; Islam et al., 2002; Mondol et al., 2006; Chen et al., 2013; Kratzenberg et al., 2014; Paravalos et al., 2014; Perez-Gallardo et al., 2014; Ramli et al., 2015; Nofuentes and Almonacid, 1998). As a result of these studies, *SR* values between 0.5 and 2.0 have been recommended depending on the chosen optimisation criterion, the climatic characteristics of the site, the inverter technology, the PV module technology, the orientation and tilt of the PV generator or the sun tracking type.

However, due to the novelty and complexity of the HCPV technology, the existing literature addressing these problems for HCPV systems is very scarce. We can find several research papers regarding inverters for HCPV which propose inverter models (Bowman et al., 2010; Carpanelli et al., 2015), analyse different inverter configurations (Kim and Winston, 2014; Rodrigo et al., 2016b) or design test procedures for the inverters (Domínguez and Voarino, 2014; Voarino et al., 2015), but these studies do not deal with the inverter sizing analysis. There are only two studies which analyse the inverter sizing in HCPV. Chen and Melia (2011) calculated the optimum inverter sizing which optimizes the financial return in 5 locations with high annual *DNI* levels in the southwest of USA, considering the Solfocus HCPV technology. These authors used the model proposed in (Dittmer and McDonald, 2009) to predict the DC power injected to the inverter, which accounts for the *DNI*, temperature and air mass as atmospheric inputs. Results recommended *SR* values around 0.8 for the case study. Martínez et al. (2016) analysed three configurations of HCPV power plants (micro-, tracker-, and central-inverters) in order to maximize the annual energy yield in Jaén, southern Spain. They predicted the DC power based on the model proposed in (Fernández et al., 2013b, 2013c), which considers the *DNI*, temperature and air mass. The recommendation in this case was to size the inverters with *SR* values around 0.9 independently of the chosen configuration, although the different configurations presented different levels of DC losses. As can be established, the existing papers do not consider the *AOD* as a relevant atmospheric variable, and are limited to particular types of HCPV generators and inverters.

## 3. HCPV system modelling

The output power of the HCPV system per kWp of installed power (rated at CSTC), $p_{sys}$, is expressed in this study as:

$$p_{sys} = p_{mod,MPP}\cdot(1-L_{DC})\cdot\eta_{inv}\cdot(1-L_{AC}) \quad (2)$$

where $p_{mod,MPP}$ is the maximum power of an HCPV module per kWp of nominal power (rated at CSTC), $\eta_{inv}$ is the inverter efficiency and $L_{DC}$, $L_{AC}$ are per unit coefficients representing the DC losses and AC losses of the HCPV system respectively.

$p_{mod,MPP}$ is influenced by *DNI*, cell temperature ($T_{cell}$) and direct sunlight spectrum (Fernández et al., 2014a; 2012; 2014c, 2013b, 2013c; Chan et al., 2013, 2014; Peharz et al., 2011; Fernández et al., 2013a). According to the model experimentally validated in (Fernández et al., 2015d, 2016b), it can be expressed as:

$$p_{mod,MPP} = \frac{DNI}{DNI_{CSTC}}\cdot[1-\delta(T_{cell}-T_{cell,CSTC})]\cdot[1-\varepsilon(AM-AM_u)]\cdot [1-\phi(AOD_{550}-AOD_{550,u})] \quad (3)$$

where the subscript "CSTC" represents the Concentrator Standard Test Conditions and the subscript "u" indicates the threshold values of air mass (*AM*) and aerosol optical depth at 550 nm ($AOD_{550}$). $\delta$ is the temperature coefficient of maximum power, similar to that commonly

employed in conventional PV systems (Evans, 1981; Osterwald, 1986), $\epsilon$ is the coefficient for calculating spectral losses due to *AM* and $\varphi$ is the coefficient for calculating spectral losses due to $AOD_{550}$. According to (Fernández et al., 2014a), the spectral impact of precipitable water (*PW*) in the power output of an HCPV module is in the range from -4% to 2%; this small influence will cause negligible integrated annual energy spectral losses and, at the end, will not affect the optimum inverter size. Because of this, the spectral influence of *PW* was not included in the spectral correction factor in Eq. (3).

In order for this expression to be used, the $T_{cell}$ of the HCPV module must be known. Among the available models for the characterization of $T_{cell}$ (Rodrigo et al., 2014; Fernández et al., 2013b, 2013c; Almonacid et al., 2012), in this study, the model developed in (Fernández et al., 2014b; Fernández and Almonacid, 2015) is used, which analytically relates $T_{cell}$ to the *DNI*, the ambient temperature ($T_{air}$) and the portion of the incident *DNI* which is transformed to heat, making use of the thermal resistance of the HCPV module ($R_{th}$).

$L_{DC}$ quantifies the following losses that take place in the HCPV generator:

- Soiling losses: due to the deposition of dirt and dust on the lens surfaces.
- Mismatch losses: due to effects such as different misalignment angles of the HCPV modules, imperfect alignment of the different receivers in each module, sun tracking inaccuracies, temperature differences across the receivers of the generator or dispersion of the electrical/optical properties of the different solar cells/concentrator optical assemblies.
- Ohmic losses: due to the voltage drop across the wires that interconnect the modules and across the wires that connect the generator to the inverter.

It is assumed that the generator is free of shadows, so that no shading losses are considered.

The global efficiency of the inverter ($\eta_{inv}$) is the quotient between the output AC power and the input DC power. HCPV systems use the same types of inverters as conventional PV systems. Although the input of the system is the direct irradiance instead of the global irradiance, and this component has faster variations in the field, no special maximum power point (MPP) trackers have been developed for HCPV. There is a type of inverter called “tracking inverter” (Stalter and Burger, 2009), which incorporates the control of the engines of the sun tracker, but it uses the same MPP trackers as conventional inverters. Thus, the existing efficiency models for conventional inverters can be used in this study. $\eta_{inv}$ is expressed by (Bletterie et al., 2011; Peippo and Lund, 1994a, 1994b):

$$\eta_{inv} = 1-(L_0 + L_1 p_{in} + L_2 p_{in}^2)/p_{in} \quad (4)$$

where $L_0$, $L_1$, $L_2$ are the inverter loss coefficients (constant self-consumption loss, loss increasing linearly with power and a loss increasing proportionally with the square of power respectively) and $p_{in}$ is the inverter input DC power normalized to the inverter nominal AC power. $p_{in}$ can be calculated from the maximum power of the HCPV generator and the sizing ratio by:

$$p_{in} = [p_{mod,MPP}\cdot(1-L_{DC})]/SR \quad (5)$$

Finally, $L_{AC}$ is the per unit coefficient representing the system AC power losses, which include AC wiring ohmic losses and transformer losses.

With the above expressions, $p_{sys}$ is calculated each 10 min. The system final energy yield in kWh/kWp ($Y_f$) is then obtained by integrating power values over one year. In addition, the annual Performance Ratio (*PR*) can be computed as the ratio of the energy yield to the annual direct normal irradiation in kWh/m$^2$ ($DNI_A$) for the site.

The criterion of maximizing the final energy yield is equivalent to the criterion of maximizing the annual *PR*. Thus, the inverter size can be optimized by finding the *SR* that maximizes the annual *PR*. This is the approach followed in the present study and has the advantage that *PR* values are easier to compare between different locations than energy yield values, given that *PR* does not depend on the $DNI_A$ of each location.

## 4. Model parameters

As was mentioned, an HCPV system basically consists of a set of HCPV modules feeding DC power to an inverter, which performs the DC/AC conversion. This study focuses on one type of HCPV module and three types of inverters (low-, medium-, and high-efficiency).

Currently, the most industrialized HCPV module is made up of triple-junction GaInP/GaInAs/Ge solar cells. One point-focus optical system per cell is used and the cells are interconnected in series. The primary optical elements are Fresnel lenses, which concentrate the sunlight on the secondary optical elements. The optical properties of the secondary optical elements allow the light to be homogenized before reaching the solar cells, as well as improving the system angular acceptance. The most commonly used materials for the Fresnel lenses are polymethylmethacrylate (PMMA) or silicone-on-glass (SOG). In this study, the parameters that characterise the HCPV module were experimentally obtained from the outdoor measurements of an HCPV generator installed at the Centro de Estudios Avanzados en Energía y Medio Ambiente (CEAEMA) of University of Jaén (southern Spain). This generator consists of 9 HCPV modules of typical characteristics and started operation in 2011. Since then, the main atmospheric and electrical parameters were recorded every minute. The generator is mounted on a two-axis sun tracker settled in open loop to the irradiance and close loop to the position, which allows a high level of tracking accuracy (an error lower than 0.1°). Further details about the experimental set-up can be found in a previous paper (Fernández and Almonacid, 2015).

On the other hand, the parameters that characterise the three types of inverters are based on the analysis of 80 commercial datasheets, covering 5 manufacturers with great presence in the market. The following two subsections explain the parameterization of the HCPV module and inverters considered.

### 4.1. Parameters of the HCPV module

The HCPV module taken as reference for the parameterization of the model consists of 25 triple-junction lattice-matched GaInP/GaInAs/Ge solar cells interconnected in series, PMMA Fresnel lenses as primary optical elements and refractive truncated pyramids as secondary optical elements. The geometric concentration ratio is 550× and the optical efficiency is 85%. The module uses passive cooling based on an aluminium plate to maintain the temperature of the solar cells within their optimum operating range (50–80 °C). The scheme of a solar receiver for the HCPV module considered is shown in Fig. 1. The external quantum efficiency of the triple-junction solar cells and the transmittance function of the PMMA Fresnel lenses as a function of the wavelength are represented in Fig. 2 (Fernández and Almonacid, 2015; Fernández et al., 2015c). The rated values of the main electrical parameters of the concentrator module under CSTC tested with the Helios 3198 solar simulator, see Fig. 3, at CEAEMA following the procedure described in (Fernández et al., 2017) are shown in Table 1.

The parameter values obtained from outdoor characterisation procedures for the HCPV module and generator considered are indicated in Table 2. It is remarkable that these values fall within the typical ranges found in the literature for the type of HCPV module under study. The temperature coefficient of power, $\delta$, typically takes values between 0.001 and 0.002 °C$^{-1}$; the *AM* coefficient, $\varepsilon$, typically takes values between 0.04 and 0.05; and, the *AOD* coefficient, $\varphi$, typically takes values

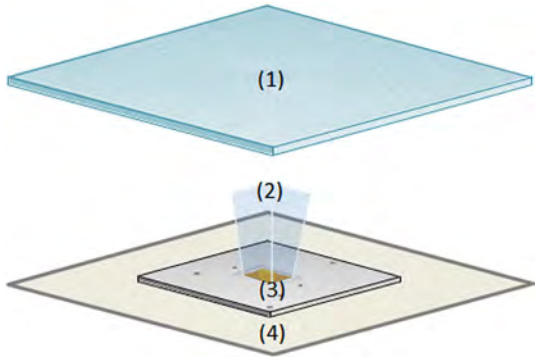


**Fig. 1.** Schematic diagram of an HCPV solar converter unit: (1) Primary optics, (2) Secondary optics, (3) Multi-junction cell and, (4) Module chassis.

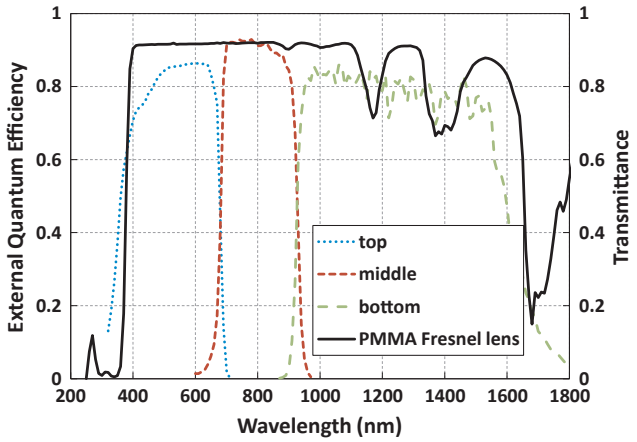


**Fig. 2.** External quantum efficiency of the triple-junction solar cells and transmittance of the PMMA Fresnel lenses for the HCPV module considered.

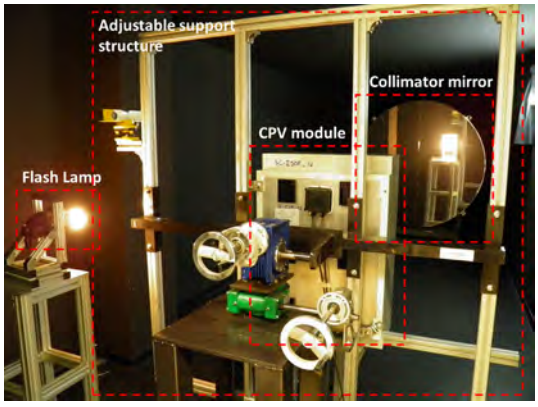


**Fig. 3.** Photo of the Helios 3198 CPV solar simulator installed at the Centro de Estudios Avanzados en Energía y Medio Ambiente (CEAEMA) of the University of Jaen.

around 0.32. Regarding the threshold values of *AM* and *AOD*, $AM_u$ typically takes values range between 1.5 and 2.5, while $AOD_{550,u}$ typically takes values range between 0.05 and 0.25 (Fernández et al., 2014a; Fernández and Almonacid, 2015; Fernández et al., 2015a). For the thermal resistance of the HCPV module, $R_{th}$, a value of 0.059 °C/W m$^{-2}$ was obtained. This value is similar to that reported in (Almonacid et al., 2012), and falls within the range obtained in (Jaus et al., 2009) for an HCPV module similar to the analysed in this study, although it is not exactly equal. As can be observed, all the HCPV module model parameters fall within the typical ranges established in the literature, which implies that the parameters are representative of the HCPV modules currently available in the market.

**Table 1**
Rated values of the main electrical parameters of the reference CPV module used in this study obtained with the Helios 3198 CPV solar simulator at the CEAEMA in the University of Jaen at 1000 W/m$^2$, spectral irradiance similar to AM1.5D reference spectrum, SMR (top/mid) = 1 ± 0.05 and room temperature of 25 °C ± 0.5 °C.

| Parameter | Value |
|---|---|
| $I_{sc}$ (A) | 2.47 |
| $I_{mpp}$ (A) | 2.08 |
| $V_{oc}$ (V) | 77.2 |
| $V_{mpp}$ (V) | 71.5 |
| $P_{max}$ (W) | 149.2 |

**Table 2**
Values of the coefficients obtained from outdoor monitored data for the HCPV module and generator considered.

| Coefficient | Value | Unit |
|---|---|---|
| $\delta$ | 0.0012 | °C$^{-1}$ |
| $\varepsilon$ | 0.041 | dimensionless |
| $AM_U$ | 2.06 | dimensionless |
| $\varphi$ | 0.32 | dimensionless |
| $AOD_{550,U}$ | 0.25 | dimensionless |
| $R_{th}$ | 0.059 | °C/W m$^{-2}$ |
| $L_{DC}$ | 0.044 | dimensionless |

The value per unit of the generator DC loss coefficient, $L_{DC}$, for the HCPV generator monitored at CEAEMA as was previously described is also shown in Table 2. A coefficient of 0.044 was obtained for this specific generator. The typical values of the DC loss coefficient can be quantified in values ranging between 0.030 and 0.100 according to various studies (Martínez et al., 2016; Rus-Casas et al., 2014; Sidrach-de-Cardona and Mora Lopez, 1999; Okello et al., 2015; Sharma and Chandel, 2013; Liu et al., 2012; Muñoz et al., 2011). It can be seen that the coefficient obtained in our generator falls within the typical range. However, it is remarkable that this range is wide, so that these DC losses can vary substantially from one generator to another. Because of this, a sensitivity analysis on the influence of the DC loss coefficient in the optimum *SR* will be developed in Section 6.

### 4.2. Parameters of the inverters

An analysis of 80 commercial inverter datasheets was carried out to identify the $L_0$, $L_1$ and $L_2$ inverter loss coefficients for three state-of-the-art types of inverters (low-, medium-, and high-efficiency). The list of analysed inverters is given in the Appendix A of this document. The nominal powers of the analysed inverters were in the range from 0.23 kW to 900 kW while the operating voltages were in the range from 23 V to 1000 V. From the collected data, it was concluded that $L_0$ ranges from 0.0009 to 0.0121, $L_1$ ranges from 0.0006 to 0.0570, and $L_2$ ranges from 0.0001 to 0.0514 for these state-of-the-art inverters. Making a deep data analysis showed that the three loss parameters follow a normal distribution. The mean values are respectively 0.0048, 0.0159 and, 0.0144 for $L_0$, $L_1$ and $L_2$, while the standard deviations are 0.0027, 0.0098 and, 0.0095 respectively (Fig. 4).

The range of values for the $L_0$, $L_1$ and $L_2$ inverter loss coefficients obtained in the present study are compared to the values found by other authors in previous studies in Table 3. This table together with Table 4 and Fig. 5 describe the state-of-the-art of the current inverter technology, and thus they can be considered an important contribution for the analysis of both conventional PV and HCPV systems. Jantsch *et al.* analysed 35 commercial inverters in 1992 (Jantsch et al., 1992); Muñoz

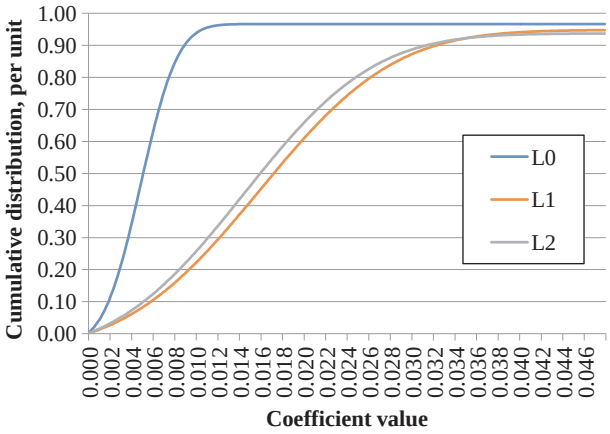


**Fig. 4.** Cumulative distribution functions of the $L_0$, $L_1$ and $L_2$ inverter loss coefficients for a set of 80 analysed commercial datasheets.

**Table 3**
Range of values obtained for the $L_0$, $L_1$ and $L_2$ inverter loss coefficients by different authors.

| Author | Year | $L_0$ | $L_1$ | $L_2$ | |
|---|---|---|---|---|---|
| This study | 2017 | 0.0009–0.0121 | 0.0006–0.0570 | 0.0001–0.0514 | (*) |
| Demoulias (2010) | 2010 | 0.0011–0.0089 | 0.0020–0.0300 | 0.0158–0.0298 | (**) |
| Muñoz et al. (2011) | 2010 | 0.0047–0.0214 | 0.0030–0.0410 | 0.0020–0.0557 | (**) |
| Jantsch et al. (1992) | 1992 | 0.0035–0.0510 | 0.0050–0.0900 | 0.0100–0.3000 | (**) |

(*) Values obtained in the present study from a set of 80 commercial inverter datasheets.
(**) Values calculated from the data published by the authors.

**Table 4**
Values of the inverter loss coefficients ($L_0$, $L_1$ and $L_2$), maximum operating efficiency ($\eta_{max}$) and range of the inverter input DC power normalized to the inverter nominal AC power in which the maximum efficiency is achieved (range $p_{in}$) for the three types of inverters considered.

| Type | $L_0$ | $L_1$ | $L_2$ | $\eta_{max}$ (%) | Range $p_{in}$ |
|---|---|---|---|---|---|
| High-efficiency | 0.0018 | 0.0057 | 0.0050 | 98.83 | 0.35–1.00 |
| Medium-efficiency | 0.0048 | 0.0159 | 0.0144 | 96.75 | 0.45–0.80 |
| Low-efficiency | 0.0088 | 0.0321 | 0.0312 | 93.47 | 0.45–0.65 |

*et al.* analysed 13 inverters with nominal power between 3.3 and 350 kW in 2010 (Muñoz et al., 2011); and, Demoulias conducted a study of 7 inverters (Solar Konzept 2 kW, Sunways 3.6 kW, SMA 5 kW, SMA 11 kW, Satcon 50 kW, Satcon 100 kW and Siemens 1000 kW) also in 2010 (Demoulias, 2010). From the values in Table 3, it is remarkable that the ranges obtained in the present study are similar to that obtained in 2010 by Demoulias and Muñoz *et al.*, but they differ from those obtained in 1992 by Jantsch *et al.*, which correspond to an older and less efficient technology.

From the analysis in Fig. 4, three typical inverters can be defined and will be used for the purposes of the current work: high-efficiency inverter, medium-efficiency inverter and low-efficiency inverter. The high-efficiency inverter is defined so that its loss coefficients ($L_0$, $L_1$ and $L_2$) have a cumulative distribution function of 10%, which corresponds to low inverter losses and therefore, to high inverter efficiency. The medium-efficiency inverter is defined so that its loss coefficients have a cumulative distribution function of 50%. Finally, the low-efficiency inverter is defined for a cumulative distribution function of 90% (high inverter losses and consequently, low inverter efficiency).

The values of the inverter loss coefficients for the three inverters considered are shown in Table 4, while the inverter efficiency curves as a function of the inverter input DC power normalized to the inverter nominal AC power ($p_{in}$) are shown in Fig. 5. From this efficiency data, it can be highlighted that the high-efficiency inverter reaches a maximum efficiency of 98.83% for $p_{in}$ approximately equal to 0.60, and keeps this value in the range of $p_{in}$ between 0.35 and 1.00 (with a deviation of less than 0.1%); the medium-efficiency inverter reaches a maximum efficiency of 96.75% for $p_{in}$ approximately equal to 0.60, and keeps this efficiency value in the range of $p_{in}$ between 0.45 and 0.80; and, the low-efficiency inverter reaches a maximum efficiency of 93.47% for $p_{in}$ approximately equal to 0.55, and keeps this value in the range of $p_{in}$ between 0.45 and 0.65. As a conclusion, as the inverter DC/AC conversion quality decreases, not only the maximum efficiency decreases, but the range of $p_{in}$ in which this maximum efficiency is achieved also narrows.

Finally, it must be mentioned that the system AC power loss coefficient ($L_{AC}$) was set in this study to 0.021, according to the value measured in the HCPV generator of CEAEMA. This value also falls within the typical range found for these kinds of systems (Fernández and Almonacid, 2015).

## 5. Locations under study and climatic characteristics

As discussed earlier, the climatic characteristics of the site influence the optimum *SR* that maximizes the system *PR*, i.e. the optimum *SR* is

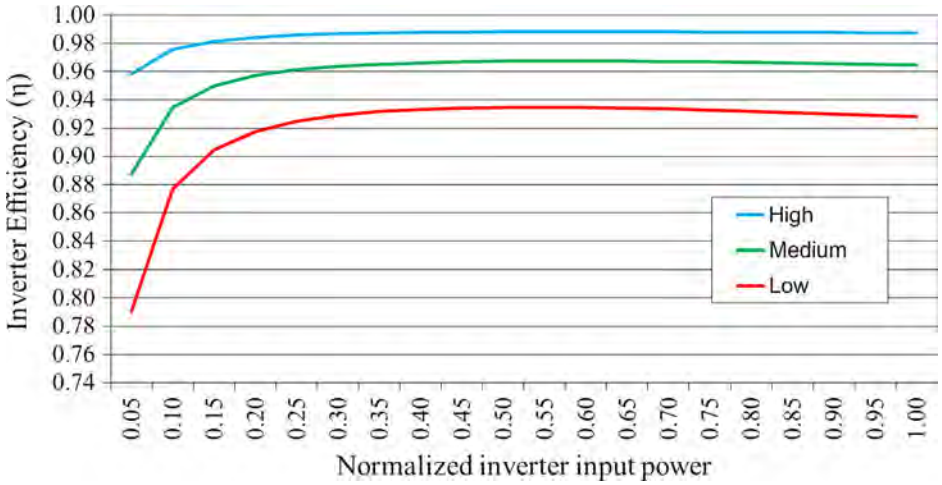


**Fig. 5.** Operating efficiency of the three inverters considered (high-, medium-, and low-efficiency) as a function of the inverter input DC power normalized to the inverter nominal AC power ($p_{in}$).

strongly related to the location under analysis. Because of this, it is desirable to apply the proposed methodology to several locations with different climates in order to analyse the influence of the local climate on the optimum *SR*.

In this study, four locations with high *DNI* levels were selected to analyse the optimum sizing of the inverter in HCPV systems. These locations are:

- Solar Village (Saudi Arabia): lat. N 24°54′25″, long. E 46°23′49″
- Alta Floresta (Brazil): lat. S 09°52′15″, long. W 56°06′14″
- Frenchman Flat (USA): lat. N 36°48′32″, long. W 115°56′06″
- Granada (Spain): lat. N 37°09′50″, long. W 03°36′18″

Although all of these worldwide sites are characterized by a high *DNI* level (and thus, all of them are appropriate for the deployment of HCPV facilities), they exhibit dissimilar average values of other relevant atmospheric variables such as $T_{air}$, *AM* and $AOD_{550}$, so that they can be used as a framework to investigate the inverter sizing of HCPV systems under a wide range of operating conditions (Fernández et al., 2014a; 2016a). These cities were selected in a previous study on the impact of spectrum and temperature in the HCPV system output (Fernández et al., 2016b). The average values of the relevant weather parameters, which characterise the selected locations, are given in Table 5.

The analytical model presented in Section 3 incorporates the most relevant atmospheric parameters influencing HCPV system performance. These atmospheric parameters (*DNI*, $T_{air}$, *AM* and $AOD_{550}$) can be obtained or calculated from atmospheric stations or databases, making the proposed methodology applicable for long-term analysis at any site with available meteorological data. In this study, input data has been obtained by the procedure previously described and validated by the authors (Fernández et al., 2015c). The *DNI* was simulated by means of the Simple Model of the Atmospheric Radiative Transfer of Sunshine (SMARTS) (Gueymard, 2001) as discussed in (Fernández et al., 2016a, 2015b; Chan et al., 2014). The *AM* was estimated from the sun's position (Kasten and Young, 1989) while the daily time-series of $AOD_{550}$ and *PW* were gathered from the Aerosol Robotic Network (AERONET) database (Holben et al., 1998; National Aeronautics and Space Administration (NASA), 2017). Finally, the time-series of $T_{air}$ was modelled from the maximum, minimum and average values obtained from National Aeronautics and Space Administration (NASA) datasets (Atmospheric Science Data Center, 2016) by using the Erbs' model (Erbs et al., 1983; Almonacid et al., 2013).

## 6. Results

### 6.1. Histograms of DC power

The described procedure was used to calculate the values of the instantaneous DC power injected to the inverter for a 1 kWp HCPV system (rated at CSTC) and for the four selected locations in 10 min intervals over a whole year. Aggregate results are shown in Figs. 6 and 7.

The histograms of DC power injected to the inverter for the 1 kWp HCPV system and for the four selected locations are represented in Fig. 6. The histograms were built by considering 100 W wide classes and calculating the percentages of occurrences of each power class over a whole year. It can be seen that every location reaches values of DC power greater than 500 W for more than 50% of the samples; these percentages are 50%, 62%, 63% and 72% for Alta Floresta, Granada, Solar Village and Frenchman Flat respectively. In addition, every location presents the highest percentage of occurrences for a high value of DC power (between 500 and 700 W); the most prominent peak is reached in Frenchman Flat in the 600–700 W class, followed by Granada in the 500–600 W class; Alta Floresta and Solar Village also present a peak in the 500–600 W class, although this peak is not as prominent as in the other two cities. The histograms reveal that the behaviour of the DC power injected to the inverter follows a different distribution in each site due to the different atmospheric conditions. This confirms that the selection of sites is appropriate for analysing a wide range of operating conditions when compared to the optimum sizing of the inverters.

The duration curves of DC power injected to the inverter for the 1 kWp HCPV system and for the four selected locations are shown in Fig. 7. These curves were conceived to represent the number of hours in a year that the inverter input power is greater than or equal to a given value. The power resolution of the curves is 10 W. It can be seen that the maximum calculated values of DC power are 891 W (Solar Village), 734 W (Frenchman Flat), 686 W (Alta Floresta) and 680 W (Granada). However, the average values of DC power depend on the shape of the duration curves; these average values are 547 W (Frenchman Flat), 518 W (Solar Village), 475 W (Granada) and 451 W (Alta Floresta). Therefore, the maximum DC power is obtained in Solar Village while the maximum average DC power is obtained in Frenchman Flat. From these graphs, it can be concluded that the distribution of percentages of occurrence of DC power are different in each location, so that the average annual efficiency of the inverter will also be different for each location, and thus, every location should verify a different value for the optimum *SR*.

It is worth mentioning that most of the reviewed authors use specific software or complex algorithms to calculate the optimum *SR* for a given location, while the methodology proposed in this paper is entirely analytical and all the model parameters are provided. This highlights the usefulness of the proposed procedure. Only Demoulias (2010) developed an analytical easy-to-use procedure, but it is based on the assumption (experimentally verified for several locations worldwide) that the duration curves of DC power are linear. This assumption was shown to be good when dealing with the global irradiance as input. However, as can be seen in Fig. 7, the duration curves based on the *DNI* as input cannot be considered linear functions, so that the procedure developed by Demoulias does not seem to be applicable for the sizing of HCPV systems.

### 6.2. Performance Ratio vs. Sizing Ratio

The *PR* of the HCPV system is plotted versus the *SR* for the four selected locations considering the three types of state-of-the-art inverters (high-, medium-, and low-efficiency) in Fig. 8. As can be observed, the behaviour of the curves is similar in all cases: from high to low values of *SR*, the *PR* first has a smooth increase until reaching a maximum and, afterwards, it has a fast decrease. The smooth increase is because the inverter is less oversized as the SR decreases and, thus, it operates less time at low load, condition which reduces the inverter efficiency. The fast decrease is because the inverter begins to be excessively undersized and, thus, it limits the output power to the nominal power in increasingly large periods of time, reducing also the overall inverter efficiency. The benefits can also be appreciated of choosing a high-efficiency inverter, which allows around 5% more *PR* than the low-efficiency inverter for a wide range of *SR* conditions.

The numerical values of the optimum *SR* that maximizes the final $Y_f$ of the HCPV system, together with the obtained maximum value of the *PR* and $Y_f$, for the four analysed sites and the three types of state-of-the-

**Table 5**
Annual average values of the main atmospheric parameters for the four sites analysed (only records taken above 10 W/m$^2$ of *DNI* were used to calculate the mean values) (Fernández et al., 2016b).

| Location | *DNI* (kWh/m$^2$ year) | *DNI* (W/m$^2$) | $T_{air}$ (°C) | *AM* | $AOD_{550}$ |
|---|---|---|---|---|---|
| Alta Floresta | 2246 | 608 | 27.7 | 2.8 | 0.28 |
| Granada | 2340 | 623 | 19.1 | 3.3 | 0.15 |
| Solar Village | 2582 | 694 | 28.8 | 3.0 | 0.35 |
| Frenchman Flat | 2776 | 704 | 18.4 | 3.3 | 0.07 |

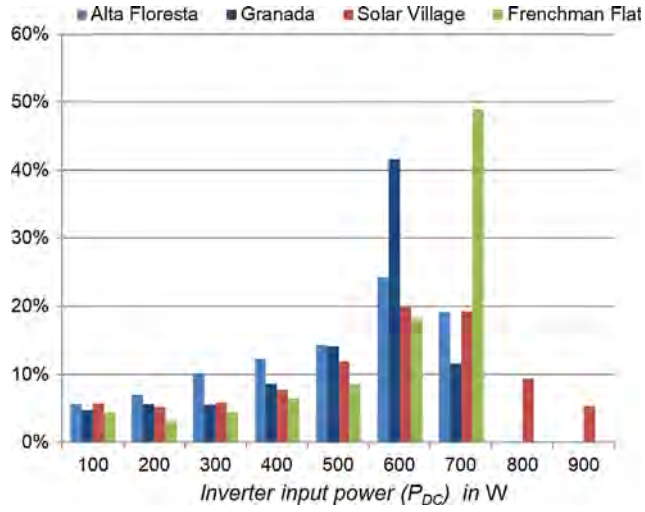


**Fig. 6.** Histograms of DC power injected to the inverter ($P_{DC}$) for a 1 kWp HCPV system (rated at CSTC) for the four selected locations. The x-axis is divided into 100 W wide classes and the y-axis shows the percentages of occurrences of each class with respect to the total number of records in a year (taken at 10 min intervals).

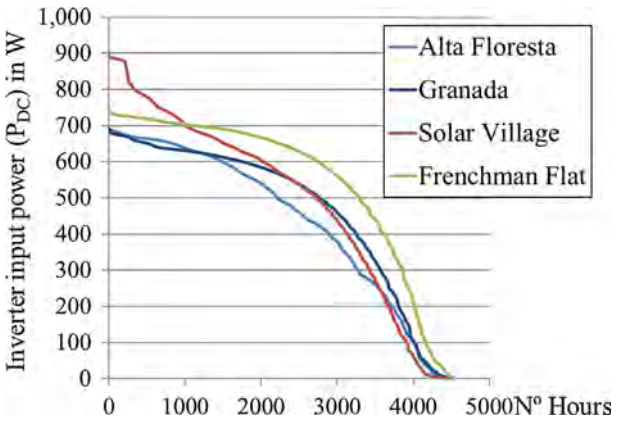


**Fig. 7.** Duration curves of DC power injected to the inverter ($P_{DC}$) for a 1 kWp HCPV system (rated at CSTC) for the four selected locations. The curves express the number of hours in a year that the inverter input power is greater than or equal to a given value.

art inverters, are shown in Table 6. It can be seen that the optimum *SR* ranges from 0.84 (Alta Floresta with high-efficiency inverter) to 1.12 (Frenchman Flat with low-efficiency inverter). This range of optimum *SR* is in a certain agreement with the values previously published and reviewed in Section 2 (SR ≈ 0.8 in Chen and Melia, 2011); *SR* ≈ 0.9 in Martínez et al., 2016). In every location, the optimum *SR* increases as the inverter efficiency level decreases; this is because a low-efficiency inverter needs to be more oversized than a high-efficiency inverter in order to operate more time in the range of its maximum efficiency (see the curves in Fig. 3 and the ranges of DC input power in Table 3: the high-efficiency inverter can be fed with more DC input power without lowering its efficiency, while the low-efficiency inverter has a narrower range for achieving maximum efficiency). On the other hand, as expected, the optimum *SR* increases as the annual *DNI* of the site increases, with the result that Frenchman Flat exhibited the greatest values of optimum SR while Alta Floresta exhibited the lowest values; this can be explained because a location with high annual *DNI* level will make the inverter operate more time in the region of high load (with lower efficiency than a location with moderate annual *DNI* level), unless the system is designed with an oversized inverter (increasing the *SR*), in which case this drop in efficiency can be avoided. The increase of the optimum *SR* with the annual *DNI* is plotted in Fig. 9 for the four sites and three types of inverters considered.

From Fig. 8, it is interesting to observe that the *PR* remains almost in its maximum value for a wide range of *SR* values. In Alta Floresta and Granada, the *PR* varies less than 1% for *SR* values between 0.64 and 1.50; in Solar Village, for *SR* values between 0.78 and 1.50; and, in Frenchman Flat, for *SR* values between 0.70 and 1.50. This highlights that, from the point of view of harvested energy, the designers can choose a wide range of *SR* values for the sizing of HCPV systems without compromising the annual energy yield. Moreover, this offers an opportunity for improving the economic profitability of their projects by lowering the *SR* (reducing the cost of inverters) while preserving a high energy yield level. Although it is not the aim of this paper to show the economic analysis of the inverter sizing, a straightforward preliminary analysis can be done based on the data obtained. For this purpose, we have defined a threshold *SR* as the *SR* located to the left of the optimum *SR*, which provides 1% lower *PR* than the maximum *PR*. This threshold *SR* represents a design condition which reduces the inverter investment cost while preserving a high value of the annual energy yield. The values of the threshold *SR* are shown in Table 7 for the set of analysed sites and types of inverters.

It can be seen that the threshold *SR* shows an appreciable dependency on the analysed site and a lesser dependence on the inverter efficiency type. The dependency on the analysed site is related to the registered periods of maximum DC power. The higher the maximum DC power levels and the higher the number of hours a year these high DC power levels take place, the higher the threshold *SR* needed to avoid an excessive loss in energy due to the "clipping" of the inverter. Because of this, the threshold *SR* is related to the leftmost value of the duration curves shown in Fig. 7. The maximum leftmost value of the duration curve is registered in Solar Village corresponding to the maximum values of threshold *SR*, followed by Frenchman Flat. Alta Floresta and Granada show a similar threshold *SR* because of similar levels of the maximum leftmost value of the duration curves. On the other hand, the threshold *SR* tends to increase as the inverter efficiency increases. This is because the "clipping" of the inverter takes place for more prolonged periods of time as the inverter efficiency increases, and thus it is necessary to slightly oversize the high-efficiency inverters to avoid an excessive loss of energy.

It is also worth mentioning that the values of *PR* obtained in Table 6 (ranging from 0.81 for Solar Village and low-efficiency inverter to 0.90 for Granada and high-efficiency inverter) fall within typical values found for HCPV systems (Pérez-Higueras et al., 2015). Also, the highest values of *PR* correspond to high-efficiency inverters and the highest values of $Y_f$ correspond to the locations with highest annual DNI levels, as expected.

### 6.3. Sensitivity of the optimum SR to the generator DC losses

The optimum *SR* shows a small variation when changing the model parameters within the ranges determined in Section 4: differences lower than 3% were obtained for the range of values of the HCPV generator parameters, keeping the DC loss coefficient ($L_{DC}$) and the AC loss coefficient ($L_{AC}$) as constants.

The range of variation of $L_{AC}$ influences the final $Y_f$ of the system. However, if this coefficient is considered as constant and independent of the system power (which can be considered true for an HCPV system that operates correctly, without failures, grid problems, etc.), this value does not affect the optimum *SR* because these AC losses take place after the inverter output.

On the other hand, as was mentioned in Section 4.1, the $L_{DC}$ coefficient can fall within a wide range of values for the state-of-the-art HCPV generator technologies (where values between 3% and 10% have been reported) and this coefficient does influence the optimum *SR* because it represents losses that take place before the inverter input. The results shown above were obtained for $L_{DC}$ = 4.4%, i.e. the DC loss

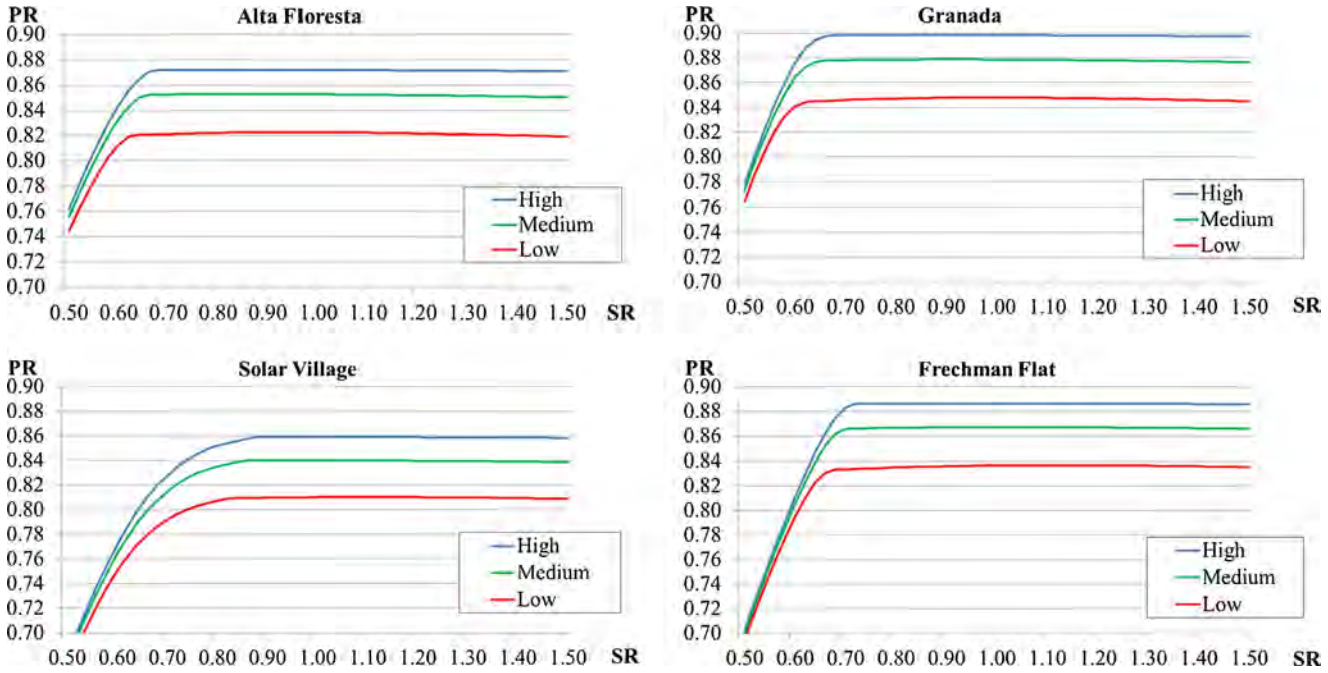


**Fig. 8.** Performance Ratio (*PR*) of the HCPV system versus Sizing Ratio (*SR*) for the four selected locations considering the three types of inverters (high-, medium-, and low-efficiency).

**Table 6**
Numerical values of the optimum Sizing Ratio (*SR*) that maximizes the final energy yield ($Y_F$) of the HCPV system for the four selected locations and the three types of inverter efficiencies. The maximum Performance Ratio (*PR*) and the maximum $Y_F$ are also shown ($Y_F$ in kWh/(kWp year), the kWp being rated at CSTC).

| | Alta Floresta | | | Granada | | | Solar Village | | | Frenchman Flat | | |
|---|---|---|---|---|---|---|---|---|---|---|---|---|
| | SR | PR | $Y_F$ | SR | PR | $Y_F$ | SR | PR | $Y_F$ | SR | PR | $Y_F$ |
| High-efficiency | **0.84** | 0.87 | 1958 | **0.88** | 0.90 | 2102 | **0.92** | 0.86 | 2218 | **0.92** | 0.89 | 2461 |
| Medium-efficiency | **0.84** | 0.85 | 1915 | **0.90** | 0.88 | 2056 | **1.00** | 0.84 | 2169 | **1.02** | 0.87 | 2407 |
| Low-efficiency | **0.94** | 0.82 | 1847 | **0.98** | 0.85 | 1984 | **1.10** | 0.81 | 2092 | **1.12** | 0.84 | 2323 |

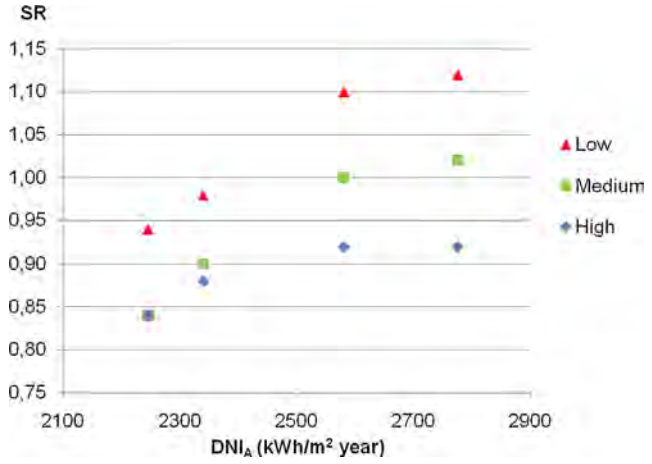


**Fig. 9.** Optimum Sizing Ratio (*SR*) versus annual Direct Normal Irradiation ($DNI_A$) for the four sites and the three types of inverters studied.

value measured in the generator monitored at CEAEMA. However, the wide range of variation of this parameter suggests performing a separate sensitivity analysis on the influence of the generator DC losses in the optimum *SR*, as the $L_{DC}$ can be considered the HCPV generator parameter with greater influence in this optimum.

The results of calculating the optimum *SR* for different values of the $L_{DC}$ coefficient (ranging from 3% to 10%), considering the four analysed

**Table 7**
Threshold Sizing Ratio for the four analysed sites and the three types of inverter efficiencies. This design parameter represents the Sizing Ratio which provides 1% lower Performance Ratio than the maximum Performance Ratio.

| | Alta floresta | Granada | Solar village | Frenchman flat |
|---|---|---|---|---|
| High-efficiency | 0.64 | 0.64 | 0.78 | 0.70 |
| Medium-efficiency | 0.64 | 0.62 | 0.78 | 0.68 |
| Low-efficiency | 0.60 | 0.60 | 0.74 | 0.66 |

locations and the three types of inverter efficiencies, are shown in Table 8. The main conclusion which can be extracted is that the optimum *SR* decreases as $L_{DC}$ increases. This is an expected result because increasing $L_{DC}$ is equivalent to decreasing the HCPV generator size and thus, a smaller inverter size is required to achieve maximum *PR*. The numerical results also show that the range of variation of $L_{DC}$ can influence the value of the optimum *SR* up to around 10%.

In order to analyse the decrease of the optimum *SR* when increasing $L_{DC}$, the following relation can be defined:

$$SR = SR_o(1 + \Delta SR) = SR_o\left(1 + \frac{\partial SR}{\partial L_{DC}} \cdot L_{DC}\right) \quad (6)$$

where $SR_o$ represents the optimum *SR* under the condition that $L_{DC} = 0$. Based on this relation, the $\Delta SR$ can be plotted versus $L_{DC}$ for the four analysed locations and the three types of inverters considered. This is done in Fig. 10, where it can be observed that the behaviour of the data can be approximated by a regression line with a correlation coefficient

**Table 8**
Optimum *SR* as a function of the DC loss coefficient ($L_{DC}$) of the HCPV generator, for the four analysed locations and the three types of inverter efficiencies (low, medium and high).

| $L_{DC}$ (%) | Alta floresta | | | Granada | | | Solar village | | | Frenchman flat | | |
|---|---|---|---|---|---|---|---|---|---|---|---|---|
| | Low | Med. | High | Low | Med. | High | Low | Med. | High | Low | Med. | High |
| 3 | 0.96 | 0.86 | 0.84 | 1.00 | 0.92 | 0.88 | 1.10 | 1.02 | 0.92 | 1.14 | 1.04 | 0.92 |
| 4 | 0.94 | 0.86 | 0.84 | 0.98 | 0.90 | 0.88 | 1.10 | 1.00 | 0.92 | 1.12 | 1.02 | 0.92 |
| 5 | 0.94 | 0.84 | 0.82 | 0.98 | 0.90 | 0.86 | 1.08 | 1.00 | 0.90 | 1.10 | 1.02 | 0.90 |
| 6 | 0.92 | 0.84 | 0.82 | 0.96 | 0.88 | 0.86 | 1.08 | 0.98 | 0.90 | 1.10 | 1.00 | 0.88 |
| 7 | 0.92 | 0.82 | 0.80 | 0.96 | 0.88 | 0.84 | 1.06 | 0.98 | 0.88 | 1.08 | 1.00 | 0.88 |
| 8 | 0.90 | 0.82 | 0.80 | 0.94 | 0.86 | 0.84 | 1.06 | 0.96 | 0.88 | 1.08 | 0.98 | 0.86 |
| 9 | 0.90 | 0.80 | 0.78 | 0.94 | 0.86 | 0.82 | 1.04 | 0.96 | 0.86 | 1.06 | 0.98 | 0.84 |
| 10 | 0.88 | 0.80 | 0.78 | 0.92 | 0.86 | 0.82 | 1.02 | 0.94 | 0.86 | 1.04 | 0.96 | 0.84 |

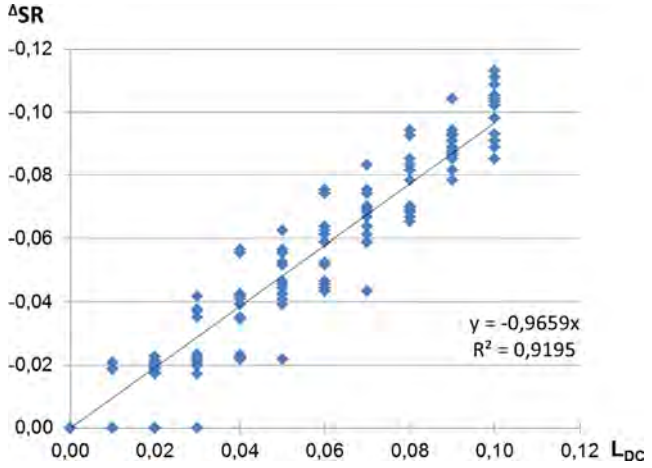


**Fig. 10.** Increase in the optimum *SR* ($\Delta SR$) versus the per unit DC loss coefficient ($L_{DC}$) for the four analysed locations and the three types of inverters considered, and results of the linear regression of the data.

$R^2$ of 0.9195. This regression analysis shows that the optimum *SR* decreases approximately 0.97% each 1% of increase of the HCPV generator DC losses.

## 7. Conclusions

The optimum *SR* that maximizes the final $Y_f$ has been studied for the state-of-the-art technology of HCPV generators and grid-connected inverters. Specifically, a typical HCPV module, three representative types of inverters (low-, medium- and high-efficiency), four locations with high annual *DNI* levels but different average values of the atmospheric parameters influencing HCPV system performance and variable DC losses of the HCPV generator have been considered in the analysis. The main results of the study can be summarized as follows:

- The optimum *SR* varies between 0.84 and 1.12.
- The optimum *SR* increases as the annual direct normal irradiation of the site increases.
- The optimum *SR* increases as the inverter efficiency decreases.
- The system *PR* remains almost in its maximum value for a wide range of *SR* values.

Therefore, from a practical point of view and considering locations with a high annual *DNI* level, designers can choose SR values between 80% and 150% without compromising the final energy yield of the system.

- The threshold *SR* that provides 1% less *PR* than the maximum *PR* varies between 0.60 and 0.78.
- The optimum *SR* decreases approximately 0.97% each 1% of increase of the HCPV generator DC losses.

Designers of HCPV systems do not have guidelines for the sizing of inverters in their projects. The literature addressing this question is very scarce and the recommendations taken from conventional PV systems are not valid for this novel technology. The main finding of this work is that they can design their systems with *SR* values between 0.60 and 0.78 according to the threshold *SR* criterion. This criterion allows reducing the cost of inverters while preserving a high system energy yield. Although the threshold *SR* depends on the climatic characteristics of the site, designers have the opportunity of implementing the methodology proposed in this paper, which consists in analytical equations, by using the parameters provided and justified in the study and feeding the algorithm with on-site atmospheric data. Furthermore, this paper presents an updated state-of-the-art for the modelling of PV grid-connected inverters, which will be useful for researchers and developers of both conventional PV systems and HCPV systems.

The results anticipate that there is a wide area of opportunity for optimising economic parameters by sizing optimization of HCPV systems. This economic analysis will be the object of future research. In addition, it is remarkable that the analysis in this paper corresponds to HCPV generators free of shadows. However, multi-tracker HCPV systems are always affected by self-shading and this effect could impact the optimum *SR* in these systems. Thus, further research is required to analyse this kind of influencing factor.

## Acknowledgment

Eduardo F. Fernández acknowledges the Spanish Ministry of Economy and Competitiveness for the Juan de la Cierva 2013 and 2015 fellowships. Pedro M. Rodrigo acknowledges the Science and Technology National Council of México (CONACYT) for the economic support as a member of the National System of Researchers. The authors also thank the Spanish Ministry of Economy and Competitiveness and FEDER funds for the projects ENE2013-45242-R and ENE2016-78251-R, and the "Plan de Apoyo a la Investigación de la Universidad de Jaén y la Caja Rural de Jaén" (UJA2015/07/01).

The authors would like to acknowledge the International AERONET Federation for providing the aerosol optical depth data used in this study.

## Appendix A

The commercial inverters analysed to obtain the coefficients that characterise the high-efficiency, medium-efficiency and low-efficiency state-of-the-art inverters are listed in Table A.1.

**Table A.1**
List of the analysed inverter models and their nominal AC power ($P_{nom}$).

| Manufacturer | Model | Pnom (W) | Manufacturer | Model | Pnom (W) | Manufacturer | Model | Pnom (W) | Manufacturer | Model | Pnom (W) |
|---|---|---|---|---|---|---|---|---|---|---|---|
| SMA | SB240-10 | 230 | SMA | SB 3000TL-21 | 3000 | SMA | SMC 7000HV-11 | 7000 | SMA | STP 15000TLEE-10 | 15,000 |
| SMA | SB1200 | 1200 | Ingecom | Sun 3,3 TL | 3300 | SMA | SMC 7000TL | 7000 | SMA | STP 15000TLHE-10 | 15,000 |
| SMA | SB1300TL-10 | 1300 | Fronius | Primo 3.5-1 | 3500 | Fronius | Symo 8.2-3-M | 8000 | SMA | STP 17000TL-10 | 17,000 |
| Fronius | Galvo 1.5-1 | 1500 | SMA | SB 3600se | 3600 | SMA | STO 8000TL-10 | 8000 | Fronius | Symo 17.5-3-M | 17,500 |
| SMA | SB1.5-1VL-40 | 1500 | SMA | SB3600TL | 3600 | SMA | STO 8000TL-20 | 8000 | Fronius | Symo 20.0-3-M | 20,000 |
| SMA | SB 1600TL-10 | 1600 | Fronius | Symo 3.7-3-S | 3700 | SMA | SMC 8000TL | 8000 | SMA | STP 20000TLEE-10 | 20,000 |
| SMA | SB 1700 | 1700 | Fronius | Symo 3.7-3-M | 3700 | Fronius | Primo 8.2-1 | 8200 | SMA | STP 20000TLHE-10 | 20,000 |
| Fronius | Galvo 2.0-1 | 2000 | Fronius | Primo 4.0-1 | 4000 | Fronius | Symo 10.0-3-M | 10,000 | SMA | STP 20000TL-30 | 20,000 |
| SMA | SB 2000HF-30 | 2000 | SMA | SB4000TL21 | 4000 | SMA | STP 10000TL-10 | 10,000 | Fronius | Eco 25.0-3-S | 25,000 |
| SMA | SB 2100TL | 2100 | Fronius | Symo 4.5-3-S | 4500 | SMA | STP 10000TLEE-JP-10 | 10,000 | Ingecom | Sun 25 kW | 25,000 |
| SMA | SB2.5-1 VL-40 | 2500 | Fronius | Symo 4.5-3-M | 4500 | SMA | STP 10000TL-20 | 10,000 | Fronius | Eco 27.0-3-S | 27,000 |
| SMA | SB 2500 | 2500 | Fronius | Symo 5.0-3-M | 5000 | SMA | SMC 10000TL-10 | 10,000 | Kaco | Powador 30 TL3 | 33,300 |
| SMA | SB 2500HF-30 | 2500 | SMA | SB 5000tl-21 | 5000 | SMA | SMC 10000TLRP-10 | 10,000 | SMA | STP 60-10 | 60,000 |
| Fronius | Symo 3.0-3-S | 3000 | SMA | STP 5000TL-20 | 5000 | SMA | SMC 11000TL-10 | 11,000 | Fronius | Agilo 75.0-3 | 75,000 |
| Fronius | Symo 3.0-3-M | 3000 | Kostal | PIKO 5.5 | 5500 | SMA | SMC 11000TLRP-10 | 11,000 | Fronius | Agilo 100.0-3 | 100,000 |
| Fronius | Primo 3.0-1 | 3000 | Fronius | Symo 6.0-3-M | 6000 | SMA | STP 12000TL-10 | 12,000 | Siemens | Sinver 100 | 100,000 |
| Fronius | Galvo 3.0-1 | 3000 | Fronius | Primo 6.0-1 | 6000 | SMA | STP 12000TL-120 | 12,000 | SMA | STP 25000TL-30 | 250,000 |
| SMA | SB 3000 | 3000 | SMA | SMC 6000TL | 6000 | Fronius | Symo 12.5-3-M | 12,500 | SMA | STP 25000TL-JP-30 | 250,000 |
| SMA | SB 3000HF-30 | 3000 | Fronius | Symo 7.0-3-M | 7000 | Fronius | Symo 15.0-3-M | 15,000 | SMA | SC 760 CP 10 | 760,000 |
| SMA | SB 3000TL-20 | 3000 | SMA | STP 7000TL-20 | 7000 | SMA | STP 15000TL-10 | 15,000 | SMA | SC 900 CP 10 | 900,000 |

## References


Almonacid, F., Pérez-Higueras, P.J., Fernández Eduardo, F., Rodrigo, P., 2012. Relation between the cell temperature of a HCPV module and atmospheric parameters. Sol. Energy Mater. Sol. Cells 105, 322–327.

Almonacid, F., Pérez-Higueras, P.J., Rodrigo, P., Hontoria, L., 2013. Generation of ambient temperature hourly time series for some Spanish locations by artificial neural networks. Renew. Energy 51, 285–291.

Atmospheric Science Data Center. (2016, 4 12). Surface meteorology and solar energy. (National Aeronautics and Space Administration (NASA)) Retrieved 6 6, 2017, from https://eosweb.larc.nasa.gov/sse/.

Bletterie, B., Bründlinger, R., Lauss, G., 2011. On the characterisation of PV inverters' efficiency - introduction to the concept of achievable efficiency. Prog. Photovol. Res. Appl. 19 (4), 423–435.

Bowman, J., Jensen, S., MacDonald, M., 2010. Inverter modeling for accurate energy predictions of tracking HCPV installations. AIP Conf. Proc. 1277 (320).

Burger, B., Rüther, R., 2006. Inverter sizing of grid-connected photovoltaic systems in the light of local solar resource distribution characteristics and temperature. Sol. Energy 80, 32–45.

Camps, X., Velasco, G., de la Hoz, J., Martín, H., 2015. Contribution to the PV-to-inverter sizing ratio determination using a custom flexible experimental setup. Appl. Energy 149, 35–45.

Carpanelli, M., Borelli, G., Verdilio, D., De Nardis, D., Migali, F., Cancro, C., Graditi, G., 2015. Characterization of the Ecosole HCPV tracker and single module inverter. AIP Conf. Proc. 1679 (120001).

Chan, N., Young, T.B., Brindley, H.E., Ekins-Daukes, N., Araki, K., Kemmoku, Y., Yamaguchi, M., 2013. Validation of energy prediction method for a concentrator photovoltaic module in Toyohashi Japan. Progr. Photovol.: Res. Appl. 21 (8), 1598–1610.

Chan, N., Brindley, H., Ekins-Daukes, N., 2014. Impact of individual atmospheric parameters on CPV system power, energy yield and cost of energy. Prog. Photovol. Res. Appl. 22 (10), 1080–1095.

Chen, X., Melia, J., 2011. Inverter size optimization for grid-connected concentrator photovoltaic (CPV) plants. 37th IEEE Photovoltaic Specialists Conference. Seattle.

Chen, S., Li, P., Brady, D., Lehman, B., 2013. Determining the optimum grid-connected photovoltaic inverter size. Sol. Energy 87, 96–116.

Demoulias, C., 2010. A new simple analytical method for calculating the optimum inverter size in grid-connected PV plants. Electr. Power Syst. Res. 80 (10), 1197–1204.

Dittmer, J., McDonald, M., 2009. Accurate energy predictions for tracking HCPV installations. 24th European Photovoltaic Solar Energy Conference. Hamburg.

Domínguez, C., Antón, I., Sala, G., Askins, S., 2013. Current-matching estimation for multijunction cells within a CPV module by means of component cells. Prog. Photovol. Res. Appl. 21, 1478–1488.

Domínguez, C., Voarino, P., 2014. CPV-specific test procedures for evaluating on-grid inverters. AIP Conf. Proc. 1616 (302).

Eltbaakh, Y.A., Ruslan, M., Alghoul, M., Othman, M., Sopian, K., Razykov, T., 2012. Solar attenuation by aerosols: An overview. Renew. Sustain. Energy Rev. 16 (6), 4264–4276.

Erbs, D.G., Klein, S.A., Beckman, W.A., 1983. Estimation of degree-days and ambient temperature bin data from monthly-average temperatures. Ashrae J. 60–65.

Evans, D.L., 1981. Simplified method for predicting photovoltaic array output. Sol. Energy 27, 555–560.

Fernández, E.F., Pérez-Higueras, P.J., Almonacid, F., García-Loureiro, A.J., Fernández, J.I., Rodrigo, P., Almonacid, G., 2012. Quantifying the effect of air temperature in CPV modules under outdoor conditions. AIP Conf. Proc. 1477, 194–197.

Fernández, E.F., Almonacid, F., Rodrigo, P., Pérez-Higueras, P.J., 2013b. Calculation of the cell temperature of a High Concentrator Photovoltaic (HCPV) module: a study and comparison of different methods. Sol. Energy Mater. Sol. Cells 121, 144–151.

Fernández, E.F., Almonacid, F., 2015. A new procedure for estimating the cell temperature of a high concentrator photovoltaic grid connected system based on atmospheric parameters. Energy Convers. Manage. 103, 1031–1039.

Fernández, E., Almonacid, F., Rodrigo, P., Pérez-Higueras, P., 2013c. Model for the prediction of the maximum power of a high concentrator photovoltaic module. Sol. Energy 97, 12–18.

Fernández, E.F., Pérez-Higueras, P.J., García Loureiro, A.J., Gómez Vidal, P., 2013a. Outdoor evaluation of concentrator photovoltaic systems modules from different manufacturers: first results and steps. Prog. Photovol. Res. Appl. 21, 693–701.

Fernández, E.F., Rodrigo, P., Fernández, J.I., Almonacid, F., Pérez-Higueras, P.J., García-Loureiro, A.J., Almonacid, G., 2014c. Analysis of high concentrator photovoltaic modules in outdoor conditions: influence of direct normal irradiance, air temperature, and air mass. J. Renew. Sustain. Energy 6 (013102).

Fernández, E.F., Almonacid, F., Ruiz-Arias, J.A., Soria-Moya, A., 2014a. Analysis of the spectral variations on the performance of high concentrator photovoltaic modules operating under different real climate conditions. Sol. Energy Mater. Sol. Cells 127, 179–187.

Fernández, E.F., Rodrigo, P., Almonacid, F., Pérez-Higueras, P., 2014b. A method for estimating cell temperature at the maximum power point of a HCPV module under actual operating conditions. Sol. Energy Mater. Sol. Cells 124, 159–165.

Fernández, E.F., Pérez-Higueras, P., Almonacid, F., Ruiz-Arias, J.A., Rodrigo, P., Fernandez, J.I., Luque-Heredia, I., 2015d. Model for estimating the energy yield of a high concentrator photovoltaic system. Energy 87, 77–85.

Fernández, E.F., Almonacid, F., Mallick, T.K., Pérez-Higueras, P.J., 2015a. Analytical modelling of high concentrator photovoltaic modules based on atmospheric parameters. Int. J. Photoenergy 2015 (872163), 1–8.

Fernández, E.F., Almonacid, F., Soria-Moya, A., Terrados, J., 2015b. Experimental analysis of the spectral factor for quantifying the spectral influence on concentrator photovoltaic systems under real operating conditions. Energy 90, 1878–1886.
Fernández, E.F., García-Loureiro, A.J., Smestad, G.P., 2015c. Multijunction concentrator solar cells: Analysis and fundamentals. Green Energy and Technology In: Pérez-Higueras, P., Fernández, E.F. (Eds.), High Concentrator Photovoltaics. Springer International Publishing, Switzerland, pp. 9–37. https://doi.org/10.1007/978-3-319-15039-0_2.
Fernández, E.F., Talavera, D.L., Almonacid, F.M., Smestad, G.P., 2016b. Investigating the impact of weather variables on the energy yield and cost of energy of grid-connected solar concentrator systems. Energy 106, 790–801.
Fernández, E.F., Soria-Moya, A., Almonacid, F., Aguilera, J., 2016a. Comparative assessment of the spectral impact on the energy yield of high concentrator and conventional photovoltaic technology. Sol. Energy Mater. Sol. Cells 147, 185–197.
Fernández, E.F., Ferrer-Rodríguez, J.P., Almonacid, F., Pérez-Higueras, P., 2017. Current-voltage dynamics of multi-junction CPV modules under different irradiance levels. Sol. Energy 155, 39–50.
Global Data, 2015. Concentrated Photovoltaic (CPV) Market, Update 2015 - Global Market Size, Competitive Landscape and Key Country Analysis to 2020.
Gueymard, C., 2001. Parameterized transmittance model for direct beam and circumsolar spectral irradiance. Sol. Energy 71 (5), 325–346.
Holben, B.N., Eck, T.F., Slutsker, I., Tanré, D., Buis, J.P., Setzer, A., Smirnov, A., 1998. AERONET - A federated instrument network and data archive for aerosol characterization. Remote Sens. Environ. 66 (1), 1–16.
Hussin, M.Z., Omar, A.M., Zain, Z.M., Shaari, S., 2012. Sizing ratio of inverter and PV array for a-Si FS GCPV system in Malaysia's perspectives. IEEE Control and System Graduate Research Colloquium (ICSGRC). Shah Alam, Selangor: IEEE Control and System Graduate Research Colloquium (ICSGRC).
IEC 62670-1:2013, 2013. Photovoltaic concentrators (CPV) – Performance testing – Part 1: Standard conditions. Edition 1.0. Geneve.
Islam, S., Woyte, A., Belmans, R., Nijs, J., 2002. Undersizing inverters for grid connection - What is the optimum? Photovoltaic in Europe. Photovoltaic, Rome (in Europe).
Jantsch, M., Schmidt, H., Schmid, J., 1992. Results of the concerted action on power conditioning and control. In: 11th European Photovoltaic Solar Energy Conference, Montreux, pp. 1589–1592.
Jaus, J., et al., 2009. Development of FLATCON® modules using secondary optics. In: 34th IEEE Photovoltaic Specialist Conference. Philadelphia, PA, USA.
Kasten, F., Young, A.T., 1989. Revised optical air mass tables and approximation formula. Appl. Opt. 28, 4735–4738.
Keller, L., Affolter, P., 1995. Optimizing the panel area of a photovoltaic system in relation to the static inverter - Practical results. Sol. Energy 55 (1), 1–7.
Kim, Y.S., Winston, R., 2014. Power conversion in concentrating photovoltaic systems: central, string, and micro-inverters. Prog. Photovol. Res. Appl. 22, 984–992.
Kratzenberg, M.G., Deschamps, E.M., Nascimento, L., Rüther, R., Zürn, H.H., 2014. Optimal photovoltaic inverter sizing considering different climate conditions and energy prices. Energy Procedia 57, 226–234.
Liu, M., Kinsey, G.S., Bagiensky, W., Nayakand, A., Garboushian, V., 2012. Measurement of mismatch loss in CPV modules. AIP Conf. Proc. 1477, 165–167.
Luoma, J., Kleissl, J., Murray, K., 2012. Optimal inverter sizing considering cloud enhancement. Sol. Energy 86, 421–429.
Macagnan, M.H., Lorenzo, E., 1992. On the optimal size of inverters for grid connected PV systems. European Photovoltaic Solar Energy Conference. Montreux: European Photovoltaic Solar Energy Conference.
Macedo, W.N., Zilles, R., 2007. Operational results of grid-connected photovoltaic system with different inverter's sizing factors (ISF). Prog. Photovol. Res. Appl. 15, 337–352.
Martínez, M., Sánchez, D., Rubio, F., Fernández, E.F., Almonacid, F., Abela, N., Gerstmaier, T., 2016. CPV Power Plants. In Handbook of Concentrator Photovoltaic Technology. Carlos Algora and Ignacio Rey-Stolle, editors. John Wiley & Sons, pp. 448–450.
Mondol, J.D., Yohanis, Y.G., Norton, B., 2006. Optimal sizing of array and inverter for grid-connected photovoltaic systems. Sol. Energy 80, 1517–1539.
Muñoz, J., Martínez-Moreno, F., Lorenzo, E., 2011. On-site characterisation and energy efficiency of grid-connected PV inverters. Prog. Photovol. Res. Appl. 19 (2), 192–201.
Muñoz, E., Muñoz-Rodríguez, F.J., de la Casa, J., Pérez-Higueras, P.J., 2015. High-concentrator photovoltaic systems configuration and. Green Energy and Technology In: Pérez-Higueras, P., Fernández, E.F. (Eds.), High Concentrator Photovoltaics. Springer International Publishing, Switzerland, pp. 209–237. https://doi.org/10.1007/978-3-319-15039-0_7.
National Aeronautics and Space Administration (NASA). (2017, 3 28). AERONET - Aerosol Robotic Network. (Goddard Space Flight Center) Retrieved 6 6, 2017, from https://aeronet.gsfc.nasa.gov/.
Nofuentes, G., Almonacid, G., 1998. An approach to the selection of the inverter for architecturally integrated photovoltaic grid-connected systems. Renew. Energy 15 (1–4), 487–490.
Nofuentes, G., Almonacid, G., 1999. Design tools for the electrical configuration of architecturally-integrated PV in buildings. Prog. Photovoltaics Res. Appl. 7, 475–488.
Notton, G., Lazarov, V., Stoyanov, L., 2010. Optimal sizing of a grid-connected PV system for various PV module technologies and inclinations, inverter efficiency characteristics and locations. Renew. Energy 35, 541–554.
Núñez, R., Jin, C., Victoria, M., Domínguez, C., Askins, S., Herrero, R., Sala, G., 2016. Spectral study and classification of worldwide locations considering several multi-junction solar cell technologies. Prog. Photovol. Res. Appl. 24 (9), 1214–1228.
Okello, D., van Dyk, E.E., Vorster, F.J., 2015. Analysis of measured and simulated performance data of a 3.2 kWp grid-connected PV system in Port Elizabeth South Africa. Energy Convers. Manage. 100, 10–15.
Osterwald, C., 1986. Traslation of device performance measurments to reference conditions. Sol. Cells 18, 269–279.
Paravalos, C., Koutroulis, E., Samoladas, V., Kerekes, T., Sera, D., Teodorescu, R., 2014. Optimal design of photovoltaic systems using high time-resolution meteorological data. IEEE Trans. Indus. Inform. 10 (4), 2270–2279.
Peharz, G., Ferrer-Rodríguez, J.P., Siefer, G., Bett, A.W., 2011. Investigations on the temperature dependence of CPV modules equipped with triple-junction solar cells. Prog. Photovol. Res. Appl. 19, 54–60.
Peippo, K., Lund, P.D., 1994b. Optimal sizing of solar array and inverter in grid-connected photovoltaic systems. Sol. Energy Mater. Sol. Cells 32, 95–114.
Peippo, K., Lund, P.D., 1994a. Optimal sizing of grid-connected PV-systems for different climates and array orientations: a simulation study. Sol. Energy Mater. Sol. Cells 35, 445–451.
Perez-Gallardo, J.R., Azzaro-Pantel, C., Astier, S., Domenech, S., Aguilar-Lasserre, A., 2014. Ecodesign of photovoltaic grid-connected systems. Renew. Energy 64, 82–97.
Pérez-Higueras, P.J., Muñoz, E., Almonacid, G., Vidal, P.G., 2011. High Concentrator Photovoltaics efficiencies: Present status and forecast. Renew. Sustain. Energy Rev. 15, 1810–1815.
Pérez-Higueras, P., Muñoz-Rodríguez, F.J., Adame-Sánchez, C., Hontoria-García, L., Rus-Casas, C., González-Rodríguez, A., Aguilar-Peña, J.D., Gallego-Álvarez, F.J., González-Luchena, I., Fernández, E.F., 2015. High-concentrator photovoltaic power plants: Energy balance and case studies. Green Energy and Technology In: Pérez-Higueras, P., Fernández, E.F. (Eds.), High Concentrator Photovoltaics. Springer International Publishing, Switzerland, pp. 443–477. https://doi.org/10.1007/978-3-319-15039-0_16.
Philipps, S.P., Bett, A.W., Horowitz, K., Kurtz, S., 2016. Current status of concentrator photovoltaic (CPV) technology, version 1.2. Fraunhofer Institute for Solar Energy Systems ISE and National Renewable Energy Laboratory (NREL).
Ramli, M.A., Hiendro, A., Sedraoui, K., Twaha, S., 2015. Optimal sizing of grid-connected photovoltaic energy system in Saudi Arabia. Renew. Energy 75, 489–495.
Rodrigo, P., Fernández, E.F., Almonacid, F., Pérez-Higueras, P.J., 2013. Models for the electrical characterization of high concentration photovoltaic cells and modules: a review. Renew. Sustain. Energy Rev. 26, 752–760.
Rodrigo, P., Fernández Eduardo, F., Almonacid, F., Pérez-Higueras, P.J., 2014. Review of methods for the calculation of cell temperature in high concentration photovoltaic modules for electrical characterization. Renew. Sustain. Energy Rev. 38, 478–488.
Rodrigo, P., Velázquez, R., Fernández, E.F., Almonacid, F., Pérez-Higueras, P.J., 2016b. Analysis of electrical mismatches in high-concentrator photovoltaic power plants with distributed inverter configurations. Energy 107, 374–387.
Rodrigo, P.M., Velázquez, R., Fernández, E.F., 2016a. DC/AC conversion efficiency of grid-connected photovoltaic inverters in central Mexico. Sol. Energy 139, 650–665.
Rodrigo, P.M., Fernández, E.F., Almonacid, F.M., Pérez-Higueras, P.J., 2017. Quantification of the spectral coupling of atmosphere and photovoltaic system performance: Indexes, methods and impact on energy harvesting. Sol. Energy Mater. Sol. Cells 163, 73–90.
Rus-Casas, C., Aguilar, J.D., Rodrigo, P., Almonacid, F., Pérez-Higueras, P.J., 2014. Classification of methods for annual energy harvesting calculations of photovoltaic generators. Energy Convers. Manage. 78, 527–536.
Shanks, K., Senthilarasu, S., Mallick, T.K., 2016. Optics for concentrating photovoltaics: Trends, limits and opportunities for materials and design. Renew. Sustain. Energy Rev. 60, 394–407.
Sharma, V., Chandel, S., 2013. Performance analysis of a 190 kWp grid interactive solar photovoltaic power plant in India. Energy 55, 476–485.
Sidrach-de-Cardona, M., Mora Lopez, L., 1999. Performance analysis of a grid-connected photovoltaic system. Energy 24, 93–102.
Stalter, O., Burger, B., 2009. Integrated solar tacker positioning unit in distributed grid-feeding inverters for CPV power plants. IEEE International Conference on Industrial Technology, Churchill, Victoria, Australia. pp. 1–5.
Talavera, D.L., Ferrer-Rodríguez, J.P., Pérez-Higueras, P.J., Terrados, J., Fernández, E.F., 2016. A worldwide assessment of levelised cost of electricity of HCPV systems. Energy Convers. Manage. 127, 679–692.
van der Borg, N.J., Burgers, A.R., 2003. Inverter undersizing in PV systems. Energy Conversion.
Velasco, G., Piqué, R., Guinjoan, F., Casellas, F., de la Hoz, J., 2010. Power sizing factor design of central inverter PV grid-connected systems: a simulation approach. International Power Electronics and Motion Control Conference. Ohrid: International Power Electronics and Motion Control Conference.
Voarino, P., Domínguez, C., Bier, A., Roujol, Y., Mangeant, C., Baudrit, M., 2015. Toward a consolidation of the CPV-specific-test procedures for inverters. AIP Conf. Proc. 1679 (030007).